Rev. Roum. Sci. Techn.– Électrotechn. et Énerg.
Vol. **71**, *2*, pp. 211–217, Bucarest, 2026

INDUCTION MOTOR BEARING FAULTS DIAGNOSIS USING AN IMPROVED KURTOGRAM METHOD

MOHAMMED-EL-AMINE KHODJA[1,2], AHMED HAMIDA BOUDINAR[2], AMEUR FETHI AIMER[3], AZEDDINE BENDIABDELLAH[2]

Keywords: Induction motor; Stator current; Rolling-elements bearing; Fault diagnosis; Spectral kurtosis; Kurtogram.

It is well known that the bearing's outer race is the most failing part of the rolling-element bearings used in induction motors, which causes, in most cases, the complete shutdown of the entire industrial process. Moreover, the early diagnosis of this fault is essential to improve the operational reliability of these motors and to avoid huge financial losses. In this aim, demodulating the stator current envelope is a promising diagnostic approach, allowing direct extraction of the fault signature without being affected by the fundamental frequency. In addition, the Kurtogram, a statistical tool of 4th order spectral analysis, makes it possible to extract the signature of the searched faults even in the case of non-stationary signals. Therefore, the purpose of this paper is to address a comparative study between two Kurtogram-based computation algorithms: Fast-Kurtogram and Wavelet-Kurtogram. The experimental results obtained by the stator current spectral analysis show the superiority of the Wavelet-Kurtogram compared to the Fast-Kurtogram in the detection and localization of the outer race fault.

1. INTRODUCTION

To ensure operational reliability of industrial processes and thus avoid financial losses, early diagnosis of electric motors, as well as precise localization of the faults affecting them, is important. Most often, the failures affecting motors are in rolling-element bearings since these elements allow the transfer of mechanical energy. Indeed, they represent 69% of induction motor failures [1–7].

It is necessary to mention that if a fault occurs on one of the rolling-element bearing parts, such as the outer race, the inner race, or the balls, this fault is characterized by a well-defined frequency and thus, called "localized bearing fault" [8, 9]. On the other hand, if a fault affects the surface of the bearing, it is called a "generalized roughness bearing fault". In this case, it is very difficult to detect because it is not indicated by a distinctive frequency [9–11]. To detect a "localized fault", the Motor Current Signature Analysis (MCSA) technique is an innovative and very promising method compared to traditional techniques, such as vibration analysis. This is explained by the amount of information contained in the stator current spectrum, the availability of this current in the control setup, as well as the simplicity of implementation of the corresponding sensors [12–14].

Furthermore, several signal processing techniques have been developed for the analysis of current signals, allowing the monitoring and diagnosis of this fault [15–21]. In the steady state, high-resolution signal processing techniques such as multiple signal classification (MUSIC) and estimation of signal parameters via rotational invariance techniques (ESPRIT) have an excellent frequency resolution, making it possible to discriminate two frequency signatures very close to each other. These methods are based on the decomposition of the analyzed signal into two subspaces: signal and noise. Nevertheless, their main drawbacks lie in the computation time and especially in the estimation of the model's order used in the signal modeling [15,16]. On the other hand, under non-stationary conditions, the use of time-frequency methods such as Short Time Fourier Transform (STFT) makes it possible to identify the signature of the searched faults under speed or load variations [17,18]. Other Time-Scale approaches, such as continuous or discrete wavelet transforms, give better results but with a prohibitive computation time and a much more complex algorithm [19–21].

Unfortunately, these methods, despite the signal's nature, give the fault signature relative to the fundamental frequency, which makes their distinction more difficult, especially in the case of incipient faults. To solve this problem, several envelope analysis methods are used to eliminate the fundamental frequency from the current spectrum, which will make it possible to enhance the harmonics characteristic of the motor and those related to an eventual fault [22–27].

In this aim, the Kurtosis method, a four-dimensional scalar-type statistical tool, reflects the characteristics of a distribution of a signal. Indeed, this scalar indicator is very effective in anomalies, failures, and fault detection in electric motors through numerical values, which express the global state of the motor. In other words, it is used in distributed fault diagnosis. Unfortunately, this indicator cannot give useful information on the fault origin. To interpret the numerical values obtained by Kurtosis in the spectral domain, a version of this approach in the spectral domain is necessary. For this, the first definition of the Spectral Kurtosis (SK) is given by Dwyer [28] to overcome the inability of the estimation of the Power Spectral Density (PSD) by Periodogram in the detection and characterization of non-stationary signals. The idea is to calculate the Kurtosis of the analyzed signal for "each frequency" to discern the non-stationary structures and indicate in which frequency bands they occur.

Another definition is given by Antoni [29] from the Wold-Cramér decomposition. To apply this definition in bearing fault detection, an STFT-based estimator is used [29,30]. It should be noted that fault detection using the estimation of SK based on the STFT is very sensitive to the choice of the sliding window's length. For this, a plot of several SKs with different sliding-window lengths is used to determine the optimal window length for the fault detection procedure. This calculation procedure is called the "Kurtogram". However, the major disadvantage of the Kurtogram calculation procedure is the prohibitive computation time because of the STFT-based estimator. To reduce this computation time, Antoni [31] proposes a fast Kurtogram calculation algorithm known as "Fast-Kurtogram" based on

[1] Electrical Engineering and Automation Department, Relizane University, Algeria.
[2] LDEE Laboratory, Department of Electrical Engineering, University of Sciences and Technology USTO, Algeria.
[3] LDEE Laboratory, Department of Electrical Engineering, University of Saida, Algeria.
Emails: mohammedelamine.khodja@univ-relizane.dz, ahmed.boudinar@univ-usto.dz,, azzedine.bendiabdellah@univ-usto.dz, ameurfethi.aimer@univ-saida.dz

DOI: 10.59277/RRST-EE.2026.2.7

a tree structure in filter banks instead of STFT. The use of these filter banks allows for a similarity with the fast Fourier transform (FFT) algorithm. The effectiveness of the fast-Kurtogram is illustrated in the detection of bearing faults by vibration analysis and stator current analysis in several works [23,31]. Other authors [32–34] use a wavelet-based Kurtogram technique called "Wavelet-Kurtogram" to avoid the effects of noise on the fault diagnosis procedure. For this purpose, Sawalhi [32] uses non-orthogonal complex Morlet wavelet-based filters to replace filter banks used in fast-Kurtogram. Unfortunately, complex Morlet wavelets present a considerable complexity in their implementation. To avoid this disadvantage, Lei [33] and Wang [34] prefer the use of the filters obtained by the wavelet packet transform (WPT) during the calculation of the wavelet-Kurtogram. The major advantage of the WPT is its fast calculation algorithm.

The effectiveness of the wavelet-Kurtogram is demonstrated in several papers [33,34] dealing with the detection of bearing faults by vibration analysis. On the other hand, in [23], the use of the stator current signal does not give satisfactory results. Indeed, Leite [23] uses Morlet's complex wavelet in the calculation of the Kurtogram, which affects the efficiency of bearing faults detection. These unsatisfactory results are related to the Morlet complex wavelet used in the wavelet Kurtogram. To detect the bearing fault using the stator current signal analysis and to improve the efficiency of wavelet-Kurtogram, it is preferable to use the WPT as in the vibration analysis.

The novelties of the wavelet-Kurtogram method used in this paper, compared to previous work, are:

- Stator current analysis instead of the vibration analysis given in references [33,34].
- Demodulation of the stator current using the Hilbert Transform before wavelet decomposition based on WPT.
- Avoiding the use of the “pre-whitening” technique.
- Demodulation of each decomposition using the Hilbert Transform before calculating the Kurtosis of each decomposition.
- The use of the Hilbert transform and the square of the decomposition, to enhance the harmonics of the fault, before plotting the spectrum of the decomposition.

To demonstrate all the merits of this new approach, a comparative study is carried out between both Kurtogram calculation algorithms: Fast-Kurtogram and wavelet-Kurtogram. For this purpose, several experimental tests are presented in this paper for the diagnosis of outer race bearing fault.

2. FREQUENCY SIGNATURE OF LOCALIZED BEARING FAULT

The rolling-element bearing plays an important role in the operation of electric motors. It allows the support and positioning of the rotor to keep the air gap small and constant, reducing friction and facilitating the rotation of the motor shaft. Unfortunately, this function makes it very vulnerable. Most often, bearings are made of chrome steel and consist of two circular races, inner and outer races. The movement of these races is ensured by bearing balls which are held equidistantly by a cage. The geometry of a ball bearing is illustrated in Fig. 1.

Several statistical studies have demonstrated that the bearing is the most vulnerable part in induction motors [2–10]. In addition, authors in [7] have shown that the failure of an outer race bearing is characterized by a specific vibrational frequency, defined as follows:

$$f_o = \frac{N_b}{2} f_r \left(1 - \frac{B_D}{C_D} \cos \beta\right), \quad (1)$$

where N_b is the ball number, B_D and C_D are respectively the diameter of the ball and the cage, β the contact angle and f_r the rotation frequency.

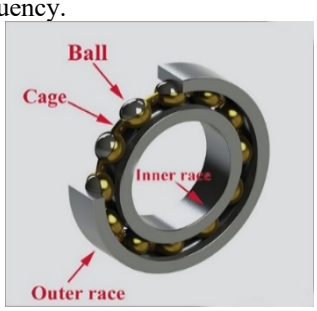

Fig. 1 – Ball bearing geometry.

3. SPECTRAL KURTOSIS AND KURTOGRAM

3.1. SPECTRAL KURTOSIS

The Spectral Kurtosis (SK) method is an improved variant of the Kurtosis scalar indicator. As its name suggests, it is used in the frequency domain to extract and localize non-stationary components of a signal. The Spectral Kurtosis (SK) method represents the normalized cumulant of order four, defined by Antoni [29] as follows:

$$SK(f) = \frac{\langle |H(n,f)|^4 \rangle}{\langle |H(n,f)|^2 \rangle^2} - 2, \quad (2)$$

where:

- $H(n,f)$ represents the complex envelope of the digitized stator current $i(n)$ at the frequency f.
- The symbol $\langle . \rangle$ represents the average value of the signal to be processed.
- 2 is a constant value. It is used in this equation instead of the constant 3 because $H(n,f)$ is a complex function.

According to [29] and [30], three important properties are considered depending on the stationarity of the signal to be processed. The SK is a constant frequency function if the signal is stationary. In addition, it is identically zero when the signal is Gaussian stationary. On the other hand, if the signal is non-stationary with stationary additive noise, the SK is expressed as follows:

$$SK_2(f) = \frac{SK_1(f)}{[1+\rho(f)]^2}, \quad (3)$$

where $\rho(f)$ represents the signal-to-noise ratio as a function of frequency. $SK_1(f)$ corresponds to the SK of the signal without noise.

Based on the three properties mentioned above, the SK is therefore capable of identifying the frequency components characterizing the searched faults, even when the motor operates under variable speed or variable load conditions.

3.2. KURTOGRAM

The Kurtogram is a fourth-order spectral analysis algorithm designed to identify non-stationary frequency components in a signal. This tool efficiently sweeps through all the frequency bands of the signal to extract the optimum band, allowing detection of the fault [30,31]. Unfortunately, this Kurtogram approach is extremely computationally

intensive and practically inapplicable in real applications, due to the total and complete exploration of all decomposition levels. To solve this problem, a fast Kurtogram computation algorithm, called fast-Kurtogram, was developed by Antoni [31].

3.2.1. FAST-KURTOGRAM

The fast-Kurtogram algorithm is based on the use of two filters allowing the filtering of the signal to be processed, followed by a subsampling operation using a factor of 2, as illustrated in Fig. 2. Where LPF is a low-pass filter, and HPF is a high-pass filter.

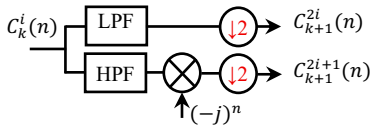

Fig. 2 – Low Pass and High Pass elementary filters.

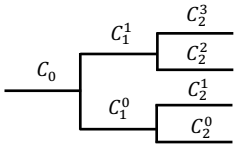

Fig. 3 – Principle of Fast-Kurtogram with a tree structure of filter banks.

A tree structure is generated by the succession of decompositions resulting from this filtering and subsampling process, as illustrated in Fig. 3. $C_k^i(n)$ represents the decomposition of the signal obtained at a k level of decomposition by the i^{th} filter, with $i = 0, \dots, 2^k - 1$. At each step of the decomposition, the corresponding Kurtosis is determined. Subsequently, the different Kurtosis K_k^i obtained are represented as an image, as illustrated in Fig. 4.

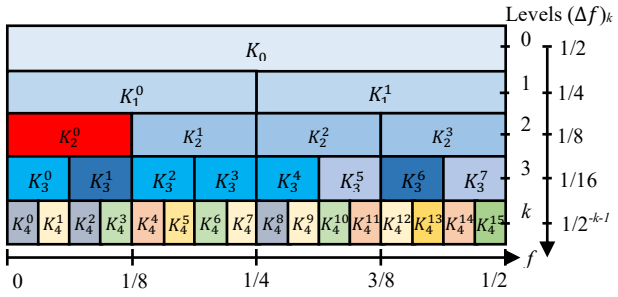

Fig. 4 – Kurtogram of the 4th level of decomposition.

Figure 4 shows that the scalar value corresponding to K_2^0 represents the maximum kurtosis for this example. Thus, the plot of the envelope of the decomposition $C_2^0(n)$, which corresponds to the maximum value (K_2^0), represents the Fast-Kurtogram. The principle is described in detail in [31]. Moreover, a band-pass filter can be defined based on the structure shown in Fig. 4, obtained from the analysis. The filter's frequency characteristics can be determined based on the decomposition to be analyzed. Thus, this filter will be characterized by a central frequency ${f_c}^i$ and a frequency band B_k as indicated in,

$$f_c^i = (i + 2^{-1})2^{-k-1}, \quad (4)$$

$$B_k = 2^{-k-1}. \quad (5)$$

For example, we obtain ${f_c}^0 = 187.5$ Hz and $B_2 = 375$ Hz for a sampling frequency of 3 kHz and the decomposition C_2^0.

3.2.2. WAVELET-KURTOGRAM

In this approach, the Kurtogram is determined using wavelet-based filters known as wavelet-Kurtogram. Sawalhi in [32] uses non-orthogonal Morlet complex wavelet-based filters. The use of this wavelet during the calculation of the Kurtogram has a considerable calculation time because of the complex programming.

Other authors [33, 34] use the WPT during the calculation of the Kurtogram based on the Daubechies wavelet using the vibration signal. The use of the WPT with this wavelet form allows speed and efficiency in fault detection [35–37]. Indeed, the Daubechies wavelet belongs to the family of orthogonal wavelets. This wavelet is characterized by a compact support with a specific number of zero moments. The mathematical form of the scale function of this wavelet is [38]:

$$\emptyset(2\pi f) = \sqrt{2}\left(\frac{1+e^{-j2\pi f}}{2}\right)^p R(2\pi f) \quad (6)$$

where p is the number of zero moments and $R(2\pi f)$ is a polynomial.

This polynomial $R(2\pi f)$ allows the Daubechies wavelet to have a faster computation time compared to the Morlet complex wavelet, which is non-orthogonal. Thus, the procedure for obtaining the wavelet-Kurtogram is the same as for the case of the fast-Kurtogram, only this time using filters based on the WPT obtained from the Daubechies wavelet.

4. EXPERIMENTAL RESULTS

A squirrel-cage induction motor, coupled to a DC generator and fed directly by the electrical network, is used during these experimental tests. The rated parameters of the induction motor are: 3 kW; 1410 rpm; 50 Hz; 4 poles. The measured signals during these tests are acquired using an acquisition chain composed of an anti-aliasing filter to avoid spectral overlap, three Hall-effect current sensors, and an acquisition card. Fig. 5 illustrates the test bench used in the experimental tests, which is connected to a computer allowing the processing of the measured signals. The rotation speed of the motor is measured using a tachometer. Furthermore, only the steady state of the current is processed under stationary conditions. Thus, this current is digitized over a period of 40 s and with a sampling time of 0.33 ms.

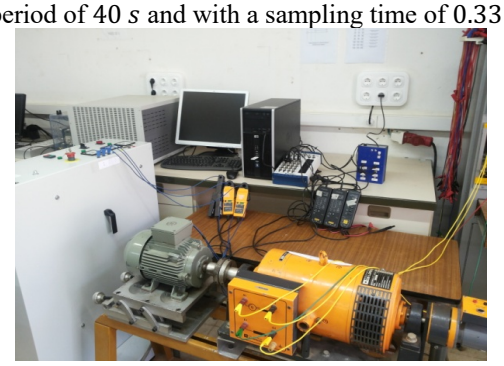

Fig. 5 – Photo of the test bench realized.

Fig. 6 – Ball bearing without and with holes on the outer race "holes of 3 mm and 6 mm diameters".

In these tests, a 6205-ZZ rolling-element bearing from the opposite side of the coupling is studied. The used bearing parameters are: $B_D = 7.835\ mm$; $C_D = 38.5\ mm$; $N_b = 9$ and $\beta = 0$. Outer race faults are simulated by creating holes with 3 mm and 6 mm diameters. The bearings used in these tests are shown in Fig. 6. Therefore, if the mechanical speed is programmed at $1435\ rpm$, corresponding to a rotation frequency of 23.9 Hz, then the signature of the outer race fault should appear around 85.72 Hz, according to (1).

The operation modes used in the diagnosis procedure are:

- Motor operation with bearings without apparent fault (without holes).
- Motor operation with an outer race fault of "3 mm" diameter.
- Motor operation with an outer race fault of "6 mm" diameter.

4.1. MOTOR OPERATION WITH BEARINGS WITHOUT APPARENT FAULTS

In this first step, the stator current is analyzed by both fast-Kurtogram and Wavelet-Kurtogram methods in the case where both bearings (coupling side and opposite side of the coupling) are without apparent fault. This analysis will be considered as the reference for other tests. For this operation mode, decomposition until level 4 is considered for both analysis methods, as shown in Fig. 7. This 4th level decomposition is obtained using eq. (5) and considering the sampling frequency used during these tests (Fe = 3 kHz).

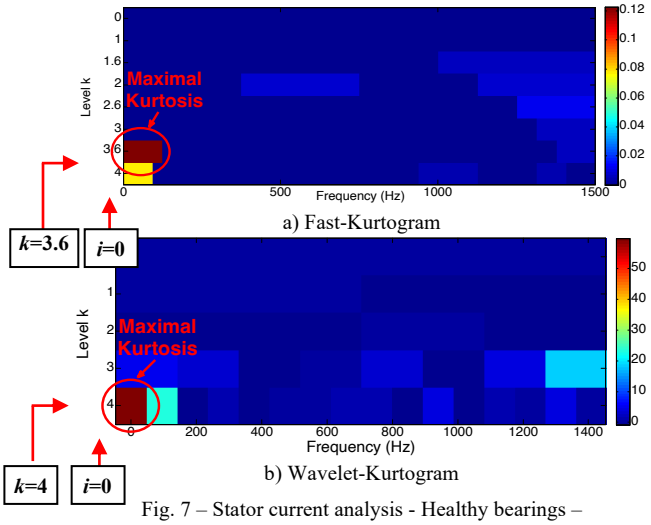

a) Fast-Kurtogram

b) Wavelet-Kurtogram

Fig. 7 – Stator current analysis - Healthy bearings –

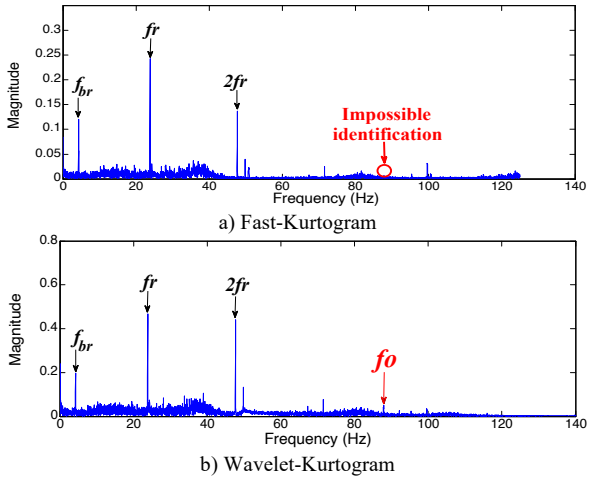

a) Fast-Kurtogram

b) Wavelet-Kurtogram

Fig. 8 – Spectral envelope of the stator current with a healthy bearing.

The maximum Kurtosis is obtained at the decomposition $C_{3.6}^0$ of the Fast-Kurtogram, as shown in Fig. 7,a. At this decomposition, a central frequency $f_c^0 = 62.5$ Hz and a frequency band $B_{3.6} = 125$ Hz are obtained. With the Wavelet-Kurtogram method, the maximum Kurtosis is obtained at the decomposition C_4^0, as shown in Fig. 7,b. A central frequency $f_c^0 = 46.875$ Hz and a frequency band $B_4 = 93.75\ Hz$ correspond to this decomposition. The spectral bands obtained by both approaches prove that the signature of the fault (85.72 Hz) is likely to appear in these spectral bands. The current envelope obtained from each decomposition of both methods is shown in Fig. 8.

From Fig. 8,a, no signature of the outer race fault is detected with the Fast-Kurtogram approach. On the other hand, it makes it possible to detect the rotation frequency of the motor and its multiples ($f_r = 23.84$ Hz and $2f_r = 47.67$ Hz) in addition to a particular frequency 4.26 Hz. We suppose that this frequency represents the signature of an imbalance of the rotor cage. Indeed, several studies [3,4] show that even a new motor may have an imbalance in its rotor cage due to the manufacturing phase. The following table proves this hypothesis.

Table 1

Frequency signatures of rotor cage imbalance.

	Theoretical Frequency $f_{br} = 2sf_s$	Real Frequency
Signature of rotor cage imbalance	4.6 Hz	4.26 Hz

where $s = 0.046$ is the motor slip and $f_s = 50$ Hz is the supply frequency.

Figure 8,b shows that the wavelet-Kurtogram detects the same frequencies obtained with fast-Kurtogram: the frequency of rotor cage imbalance f_{br} and the rotation frequency and its multiples (f_r and $2f_r$). Moreover, this method allows the detection of a low amplitude harmonic 0.0497 A/Hz at the frequency of $f_o = 87.93$ Hz. The obtained frequency corresponds to the signature of an outer race fault with a slight difference compared to the theoretical frequency calculated from (1). This difference is due to frequency resolution errors and to the accuracy of the mechanical speed measurement using the tachometer.

Although the bearing used has no apparent fault, the analysis carried out shows the presence of a low-frequency signature indicating an anomaly in the outer race. This result is certainly the consequence of the presence of scratches in this part of the bearing which is very exposed to incidents during the assembly or disassembly of this element. The results obtained highlight the superiority of the diagnosis using the Wavelet-Kurtogram method compared to the fast-Kurtogram.

4.2. MOTOR OPERATION WITH AN OUTER RACE FAULT OF "3 mm" DIAMETER

In this test, and for the same rotation speed 1435 rpm as for the 1st test, a bearing with a 3 mm hole in the outer race is used. Thus, Fig. 9.a and Fig. 9.b show respectively the results obtained by Fast-Kurtogram and Wavelet-Kurtogram for the same level of decomposition. According to these two figures, the maximum Kurtosis is obtained in the same places as in the previous case, *i.e.*, $C_{3.6}^0$ for the Fast-Kurtogram and C_4^0 for the Wavelet-Kurtogram. According to Fig. 9 a significant change in color levels is observed compared to the healthy case. This change in color levels can be considered an indicator of the presence of faults, as reflected

in the spectral content of the measured current.

The spectral analysis of the envelope of the current obtained from both decompositions ($C_{3.6}^0$ et C_4^0) is illustrated in Fig. 10. We note that the fast-Kurtogram method still allows for the detection f_r of its multiples ($2f_r$,.., as well as the signature of the rotor cage imbalance f_{br}. It is clear, based on Fig. 10.a, that the Fast-Kurtogram method is unable to detect the signature of the outer race fault. However, this fault signature is well shown with the Wavelet-Kurtogram method. Indeed, according to Fig. 10.b, the presence of the outer race fault is located at the frequency $f_o = 87.53$ Hz with an amplitude of 0.1163 A/Hz. This amplitude is much higher than that obtained during the first test without an apparent fault. This increase in the harmonic amplitude proves that the magnitude of the fault is higher. These results highlight once again the superiority of the wavelet-Kurtogram method compared to the fast-Kurtogram.

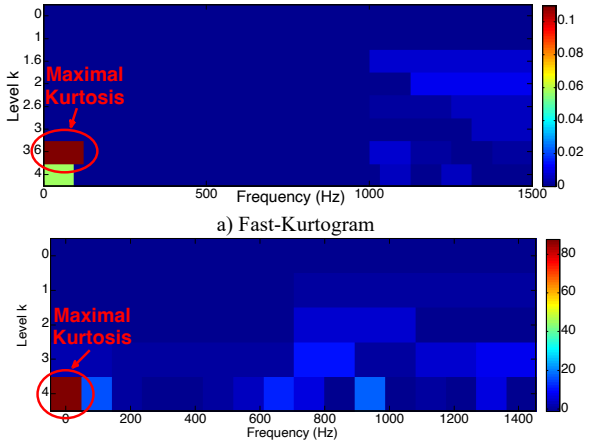

a) Fast-Kurtogram

b) Wavelet-Kurtogram

Fig. 9 – Stator current analysis – outer race fault "3 mm hole"-

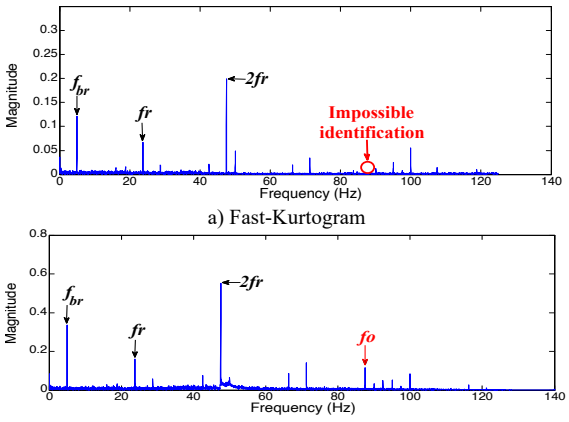

a) Fast-Kurtogram

b) Wavelet-Kurtogram

Fig. 10 – Spectral envelope of the stator current with a fault of the outer race "3 mm hole".

Note also that the spectrum obtained by both methods has more harmonics compared to the healthy case. Moreover, it is noted for this operation mode that the magnitude of the harmonic $2f$ is higher than that of the first harmonic f_r. This shows the impact of a mechanical fault on the magnitudes of these frequencies.

4.3. MOTOR OPERATION WITH AN OUTER RACE FAULT OF "6 mm" DIAMETER

For the last test, a bearing with a 6 mm hole in the outer race is used, while keeping the same rotation speed 1435 rpm. The analysis of the stator current for this test using both approaches is performed at the 4th level of the decomposition, as shown in Fig. 11.

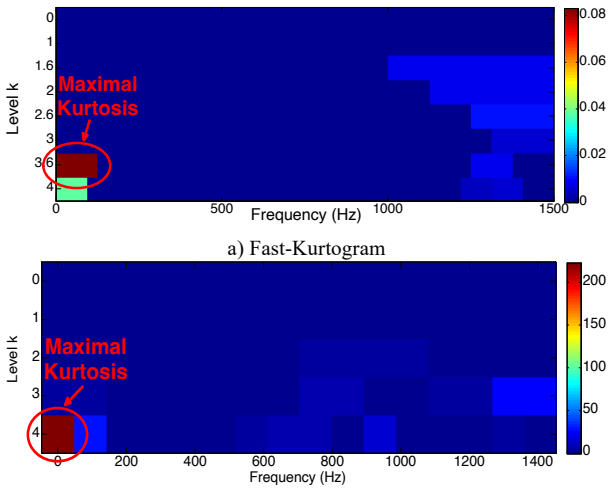

a) Fast-Kurtogram

b) Wavelet-Kurtogram

Fig. 11 – Stator current analysis – outer race fault "6 mm hole"-

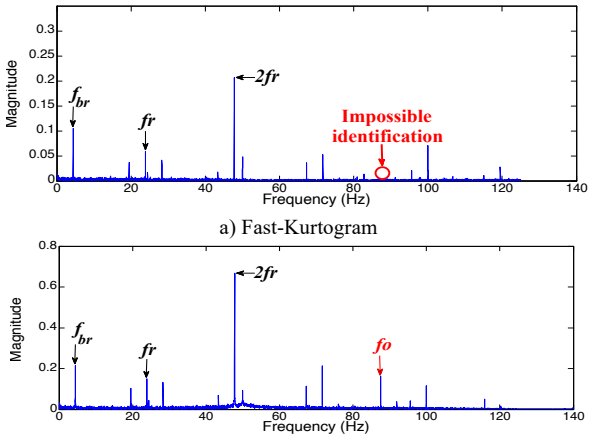

a) Fast-Kurtogram

b) Wavelet-Kurtogram

Fig. 12 – Spectral envelope of the stator current with a fault of the outer race "6 mm hole".

Indeed, we can notice that the maximum Kurtosis is obtained at $C_{3.6}^0$ for the Fast-Kurtogram and at C_4^0 for the Wavelet-Kurtogram. The spectral analysis of the current envelope from the Fast-Kurtogram method reveals the harmonics of the rotation speed f_r, $2f_r$ and that of the rotor cage imbalance frequency f_{br}, as shown in Fig. 12,a. Unfortunately, this method fails to detect the signature of the outer race fault, even for this case where the hole diameter is larger (6 mm). On the other hand, the Wavelet-Kurtogram method achieves the detection and localization with precision of the outer race fault signatures (87.53 Hz ; 0.1620 A/Hz), as well as the other frequencies f_r, $2f_r$ and f_{br}, as illustrated in Fig. 12,b.

Table 2

Monitoring of the severity of the outer race fault

Different operating modes	Bearing without hole	Outer race "3 mm hole"	Outer race "6 mm hole"
Outer race fault signature	87.93 Hz 0.0497 A/Hz	87.53 Hz 0.1163 A/Hz	87.53 Hz 0.1620 A/Hz

A thorough analysis of the evolution of the magnitude of the outer race fault signature according to the size of the hole proves that the Wavelet-Kurtogram method allows for monitoring the severity of this fault, as shown in Table 2.

5. CONCLUSION

The experimental results obtained in this paper indicate clearly that the Wavelet-Kurtogram method has a better discrimination ability and is more reliable compared to the Fast-Kurtogram method in the outer race fault diagnosis. The solution proposed in this paper, which consists of using the Daubechies wavelet, has made the Wavelet-Kurtogram method more efficient. Indeed, this method improved the readability and the analysis of the stator current spectrum. Also, the proposed method enabled the verification of the correlation between the frequency signatures of the bearing faults obtained experimentally and those computed theoretically.

CREDIT AUTHORSHIP CONTRIBUTION STATEMENT

All authors contributed equally to this work. They jointly conducted the developed proposed method, performed the experimental validation, analyzed the results, and prepared the final manuscript.

REFERENCES

1. A.H. Bonnett, C. Yung, *Increased efficiency versus increased reliability*, IEEE Ind. Appl. Mag., **14**, *1*, pp. 29–36 (2008).
2. C.Y. Lee, T.A. Le, C.L. Hung, *A feature selection approach based on memory space computation genetic algorithm applied in bearing fault diagnosis model*, IEEE Access, **11**, pp. 51282–51295 (2023).
3. A. Mohammed, S. Djurović, *Electric machine bearing health monitoring and ball fault detection by simultaneous thermo-mechanical fiber optic sensing*, IEEE Transactions on Energy Conversion, **36**, *1*, pp. 71–80 (2021).
4. J. Thankaswamy, M. Paramasivan, M. Rathinam, U.M. Sundaram, *Chaotic randomized space vector pulse width modulation intended for induction motor drives in industrial applications*, Rev. Roum. Sci. Techn. – Électrotechn. et Énerg., **69**, *4*, pp. 401–406 (2024).
5. C.V. Suru, A. Bitoleanu, M. Popescu, M. Linca, F. Ravigan, *Particularities of rotor field orientation control implementation on industrial DSP systems*, Rev. Roum. Sci. Techn. – Électrotechn. et Énerg., **70**, *1*, pp. 15–20 (2025).
6. E.G. Boudissa, M. Bounekhla, F. Habbi, *Enhanced spiral dynamic algorithm with application to induction motor parameters identification*, Rev. Roum. Sci. Techn. – Électrotechn. et Énerg., **70**, *4*, pp. 441–446 (2025).
7. E. Elbouchikhi, V. Choqueuse, Y. Amirat, M.E.H. Benbouzid, S. Turri, *An efficient Hilbert–Huang transform-based bearing faults detection in induction machines*, IEEE Transactions on Energy Conversion, **32**, *2*, pp. 401–413 (2017).
8. W. Zhou, T.G. Habetler, R.G. Harley, *Bearing fault detection via stator current noise cancellation and statistical control*, IEEE Trans. Ind. Electron., **55**, *12*, pp. 4260–4269 (2008).
9. L. Frosini, E. Bassi, *Stator current and motor efficiency as indicators for different types of bearing faults in induction motors*, IEEE Trans. Ind. Electron., **57**, *1*, pp. 244–251 (2010).
10. F. Immovilli, M. Cocconcelli, A. Bellini, R. Rubini, *Detection of generalized-roughness bearing fault by spectral-kurtosis energy of vibration or current signals*, IEEE Trans. Ind. Electron., **56**, *11*, pp. 4710–4717 (2009).
11. M. Blodt, P. Granjon, B. Raison, G. Rostaing, *Models for bearing damage detection in induction motors using stator current monitoring*, IEEE Trans. Ind. Electron., **55**, *4*, pp. 1813–1822 (2008).
12. C.Y. Lee, T.A. Le, Y.T. Lin, *A feature selection approach hybrid grey wolf and heap-based optimizer applied in bearing fault diagnosis*, IEEE Access, **10**, pp. 56691–56705 (2022).
13. M.E.A. Khodja, A.H. Boudinar, A.F. Aimer, A. Bendiabdellah, *Outer race fault diagnosis by comparison between the power spectral density and the Kurtogram*, 2019 International Aegean Conference on Electrical Machines and Power Electronics (ACEMP) & 2019 International Conference on Optimization of Electrical and Electronic Equipment (OPTIM), Turkey, pp. 254–259 (2019).
14. D. Neupane, Y. Kim, J. Seok, *Bearing fault detection using scalogram and switchable normalization-based CNN (SN-CNN)*, IEEE Access, **9**, pp. 88151–88166 (2021).
15. X. Boqiang, S. Liling, X. Lie, X. Guoyi, *Improvement of the Hilbert method via ESPRIT for detecting rotor fault in induction motors at low slip*, IEEE Trans. on Energy Conversion, **28**, *1*, pp. 225–233 (2013).
16. A.H. Boudinar, N. Benouzza, A. Bendiabdellah, M.E.A. Khodja, *Induction motor bearing fault analysis using a Root-MUSIC method*, IEEE Transactions on Industry Applications, **52**, *5*, pp. 3851–3860 (2016).
17. A.F. Aïmer, A. Boudinar, N. Benouzza, A. Bendiabdellah, *Simulation and experimental study of induction motor broken rotor bars fault diagnosis using stator current spectrogram*, Proc. of IEEE 3rd International Conference on Control, Engineering & Information Technology (CEIT), pp. 1–6 (2015).
18. H. Wang, P. Chen, *Fuzzy diagnosis method for rotating machinery in variable rotating speed*, IEEE Sensors Journal, **11**, pp. 23–34 (2011).
19. A. Ghods, H.H. Lee, *A frequency-based approach to detect bearing faults in induction motors using discrete wavelet transform*, IEEE International Conference on Industrial Technology (ICIT), Busan, pp. 121–125 (2014).
20. A. Bouzida, et al., *Fault diagnosis in industrial induction machines through discrete wavelet transform*, IEEE Trans. Ind. Electron., **58**, *9*, pp. 4385–4395 (2011).
21. J. Pons-Llinares, J.A. Antonino-Daviu, M. Riera-Guasp, M. Pineda-Sanchez, V. Climente-Alarcon, *Induction motor diagnosis based on a transient current analytic wavelet transform via frequency B-splines*, IEEE Trans. Ind. Electron., **58**, *5*, pp. 1530–1544 (2011).
22. R. Puche-Panadero, M. Pineda-Sanchez, M. Riera-Guasp, J. Roger-Folch, E. Hurtado-Perez, J. Perez-Cruz, *Improved resolution of the MCSA method via Hilbert transform, enabling the diagnosis of rotor asymmetries at very low slip*, IEEE Transactions on Energy Conversion, **24**, *1*, pp. 52–59 (2009).
23. V.C.M.N. Leite, et al., *Detection of localized bearing faults in induction machines by spectral kurtosis and envelope analysis of stator current*, IEEE Transactions on Industrial Electronics, **62**, *3*, pp. 1855–1865 (2015).
24. R.B. Randall, *Vibration-based condition monitoring: Industrial, aerospace and automotive applications*, Wiley, Chichester, U.K., pp. 167–227 (2011).
25. F. Immovilli, et al., *Diagnosis of bearing faults in induction machines by vibration or current signals: A critical comparison*, IEEE Trans. Ind. Appl., **46**, *4*, pp. 1350–1359 (2010).
26. W. Sui, D. Zhang, *Research on envelope analysis for bearing fault detection*, Proc. ICCSE, Hefei, China, pp. 973–976 (2010).
27. M. Pineda-Sanchez, et al., *Application of the Teager–Kaiser energy operator to the fault diagnosis of induction motors*, IEEE Transactions on Energy Conversion, **28**, *4*, pp. 1036–1044 (2013).
28. R.F. Dwyer, *Detection of non-Gaussian signals by frequency domain kurtosis estimation*, Proc. IEEE ICASSP, **8**, pp. 607–610 (1983).
29. J. Antoni, *The spectral kurtosis: a useful tool for characterizing nonstationary signals*, Mechanical Systems and Signal Processing, **20**, *2*, pp. 282–307 (2006).
30. J. Antoni, R. Randall, *The spectral kurtosis: application to the vibratory surveillance and diagnostics of rotating machines*, Mechanical Systems and Signal Processing, **20**, *2*, pp. 308–331 (2006).
31. J. Antoni, *Fast computation of the Kurtogram for the detection of transient faults*, Mech. Syst. Signal Process, **21**, 1, pp. 108–124 (2017).
32. N. Sawalhi, *Rolling element bearings: Diagnostic, prognostic and fault simulations*, Ph.D. dissertation, Faculty of Engineering, Mechanical and Manufacturing Engineering, University of New South Wales, Sydney, Australia, pp. 1–200 (2007).
33. Y. Lei, J. Lin, Z. He, Y. Zi, *Application of an improved Kurtogram method for fault diagnosis of rolling element bearings*, Mechanical Systems and Signal Processing, **25**, pp. 1738–1749 (2011).
34. D. Wang, P.W. Tse, K.L. Tsui, *An enhanced Kurtogram method for fault diagnosis of rolling element bearings*, Mechanical Systems and Signal Processing, **35**, pp. 176–199 (2013).
35. J.A. Antonino-Daviu, J. Pons-Llinares, S.B. Lee, *Advanced rotor fault diagnosis for medium-voltage induction motors via continuous transforms*, IEEE Transactions on Industry Applications, **5**, *5*, pp. 4503–4509 (2016).
36. S.F. Rabbi, M.L. Little, S.A. Saleh, M.A. Rahman, *A novel technique using multiresolution wavelet packet decomposition for real-time diagnosis of hunting in line start IPM motor drives*, IEEE Transactions on Industry Applications, **53**, *3*, pp. 3005–3019 (2017).
37. M.M. Rahman, M.N. Uddin, *Online unbalanced rotor fault detection of an IM drive based on both time and frequency domain analyses*, IEEE Transactions on Industry Applications, **53**, *4*, pp. 4087–4096 (2017).
38. M. Stéphane, *A wavelet tour of signal processing, the sparse way*, Academic Press, Burlington, pp. 1–400 (2009).